AChBP Engineered to Mimic the α4-α4 Binding Pocket in α4β2 Nicotinic Acetylcholine Receptors Reveals Interface Specific Interactions Important for Binding and Activity*

Azadeh Shahsavar, Philip K. Ahring, Jeppe A. Olsen, Christian Krintel, Jette S. Kastrup, Thomas Balle and Michael Gajhede

Department of Drug Design and Pharmacology, Faculty of Health and Medical Sciences, University of Copenhagen, Universitetsparken 2, 2100 Copenhagen, Denmark (A.S., J.A.O., C.K., J.S.K., M.G.); Faculty of Pharmacy, A15, The University of Sydney, NSW 2006, Australia (P.K.A., J.A.O., T.B.); Saniona AB, Baltorpvej 154, 2750 Ballerup, Denmark (P.K.A.); NeuroSearch A/S, Strandvejen 60, 2900 Hellerup, Denmark (J.A.O.)

MOL #98061

Running title: *Engineered Ls-AChBP with an α4-α4 binding pocket*

Corresponding authors:

Michael Gajhede

Department of Drug Design and Pharmacology, Faculty of Health and Medical Sciences, University of Copenhagen, Universitetsparken 2, 2100 Copenhagen, Denmark

Telephone: +45 35336407

Email: mig@sund.ku.dk

Thomas Balle

Faculty of Pharmacy, A15, The University of Sydney, NSW 2006, Australia

Telephone: +61 (0)2 90367035

Email: thomas.balle@sydney.edu.au

Number of text pages: 15

Number of tables: 3

Number of figures: 7

Number of references: 46

Number of words in the Abstract: 239

Number of words in the Introduction: 686

Number of words in the Discussion: 1482

The abbreviations used are: ACh, acetylcholine; AChBP, acetylcholine binding protein; CRR, concentration response relationship; *Ls*-AChBP, *Lymnaea stagnalis* acetylcholine binding protein; nAChR, nicotinic acetylcholine receptor; wt, wild-type.

MOL #98061

Abstract

Neuronal α4β2 nicotinic acetylcholine receptors are attractive drug targets for psychiatric and neurodegenerative disorders and smoking cessation aids. Recently, a third agonist binding site between two α4 subunits in the (α4)$_3$(β2)$_2$ receptor sub-population was discovered. In particular, three residues, H142, Q150, and T152, were demonstrated to be involved in the distinct pharmacology of the α4-α4 *vs.* α4-β2 binding sites. To obtain insight into the 3-dimensional structure of the α4-α4 binding site, a surrogate protein reproducing α4-α4 binding characteristics was constructed by introduction of three point mutations, R104H, L112Q, and M114T, into the binding pocket of *Lymnaea stagnalis* acetylcholine binding protein (*Ls*-AChBP). Co-crystallization with two agonists possessing distinct pharmacological profiles, NS3920 and NS3573, highlights the roles of the three residues in determining binding affinities and functional properties of ligands at the α4-α4 interface. Confirmed by mutational studies, our structures suggest a unique ligand-specific role of residue H142 on the α4 subunit. In the co-crystal structure of the mutated *Ls*-AChBP with the high efficacy ligand NS3920, the corresponding histidine forms an inter-subunit bridge that reinforces the ligand-mediated interactions between subunits. The structures further reveal that the binding site residues gain different and ligand-dependent interactions that could not be predicted based on wild-type *Ls*-AChBP structures in complex with the same agonists. The results show that an unprecedented correlation between binding in engineered AChBPs and functional receptors can be obtained and provide new opportunities for structure-based design of drugs targeting specific nAChR interfaces.

Introduction

The α4β2 subtype of the nicotinic acetylcholine receptor (nAChR) is the most abundant nAChR in the

brain and it is implicated in psychiatric and neurodegenerative disorders as well as in nicotine addiction,

which makes it a highly interesting therapeutic target (Jensen et al., 2005; Taly et al., 2009). The receptor

is known to assemble in two alternate stoichiometries, $(α4)_3(β2)_2$ and $(α4)_2(β2)_3$ (Fig. 1A). Interestingly,

this has been shown to influence agonist sensitivities (Nelson et al., 2003; Moroni et al., 2006; Carbone et

al., 2009; Zwart et al., 2008) and calcium ion permeability (Tapia et al., 2007) and cause distinctly

different pharmacology (Nelson et al., 2003; Kuryatov et al., 2005; Moroni et al., 2006; Tapia et al., 2007;

Moroni et al., 2008). The two receptor stoichiometires were recently found to differ in the number of

agonist binding sites. In addition to two identical sites in the interface between α4 and β2 subunits (α-β

interfaces) (Fig. 1A), common to both isoforms, the receptor with 3α:2β stoichiometry contains a third

unique agonist binding site in the interface between two α4 subunits (α-α) (Harpsøe et al., 2011). The

presence of both α-β and α-α binding sites in the 3α:2β receptor results in biphasic concentration response

relationships (CRRs) for acetylcholine (ACh) and many other agonists. This is simply because they have

different functional potencies at the two types of binding sites and occupation of all three sites is

necessary for full receptor activation. Recently, we have shown that three residues, H142, Q150, and

T152 on the complementary side of the α4 subunit (α4(-)) and V136, F144 and L146 on the

corresponding side of β2 (β2(-)) comprise the difference between the core of α-α and α-β binding sites,

respectively, and are accountable for differences in agonist sensitivities (Harpsøe et al., 2011) and agonist

binding affinities between the two sites (Ahring et al., 2015). Further, we have shown that a modulator

that selectively targets the α-α binding site may substitute for one of the agonist molecules to aid

activation *via* an agonist-like mechanism (Olsen et al., 2014a). All in all, these unique features of the α-α

site makes it particularly desirable to study to aid in design of new interface-specific drug molecules.

To understand the structural details of the α-α binding site, high-resolution structures of receptors

presenting detailed information on the specific ligand-receptor interactions are required. However, such

structures are not available and despite emerging insight from X-ray structures of full-length ligand gated

ion channels (Hilf and Dutzler, 2008; Hilf and Dutzler, 2009; Bocquet et al., 2009; Sauguet et al., 2013; Hibbs and Gouaux, 2011; Miller and Aricescu, 2014; Hassaine et al., 2014; Althoff et al., 2014), soluble ACh binding proteins (AChBPs) remain the proteins of choice when it comes to high resolution structural studies of nAChR ligand-receptor interactions (Brejc et al., 2001; Celie et al., 2004; Hansen et al., 2005; Rohde et al., 2011; Shahsavar et al., 2012). The *Lymnaea stagnalis* acetylcholine binding protein (*Ls*-AChBP) has been particularly useful as a model for the α4β2 nAChR and has provided insight into binding mode of numerous α4β2 ligands (Celie et al., 2005; Rohde et al., 2011; Shahsavar et al., 2012; Ussing et al., 2013; Olsen et al., 2014a; Olsen et al., 2014b). *Ls*-AChBP is superior to AChBPs from other species because it contains a set of five conserved aromatic residues that are present in all nAChR agonist-binding sites and that are known to play a crucial role in accommodating the positive charge of common agonists. However, despite this intact "aromatic box", the *Ls*-AChBP agonist binding site still differs from that in α-β and α-α sites by three first shell residues, R104, L112, and M114 on the complementary subunit interface, which, notably, correspond to the three residues that also differ between α-β and α-α sites and determine their functional fingerprints.

In the present study, we have investigated structural determinants of the α-α binding site to learn what governs agonist binding and functional responses. We introduced the three α-α site "signature" residues in *Ls*-AChBP (*Ls*-AChBP^{HQT}) and conducted radioligand binding experiments. The derived ligand affinities were then correlated to α-α affinities obtained from a functional α4β2 receptor in which α-β sites were engineered to resemble α-α sites by mutation of the three signature residues in the β2 subunit (α4β2^{HQT}) to ease detection of α-α binding (Ahring et al., 2015). Next, we determined crystal structures of complexes between *Ls*-AChBP^{HQT} and the α4β2 agonists NS3920 and NS3573 (Fig. 1*B*), two compounds that have distinctly different pharmacological profiles on $(\alpha4)_3(\beta2)_2$ and $(\alpha4)_2(\beta2)_3$ receptors. Based on the structures, and supported by mutational analysis, functional differences between the ligands could be attributed to their different interactions with residues in the α-α *vs.* α-β binding sites (Fig. 1*C*). The results point towards a unique ligand-specific role of the α4 residue H142 and confirm that AChBPs engineered

MOL #98061

to resemble individual binding sites have a future role in interpretation of structure activity relationships and as structural tools in drug discovery.

MATERIALS AND METHODS

Materials- NS3531 (1-(pyridin-3-yl)-1,4-diazepane), NS3573 (1-(5-ethoxypyridin-3-yl)-1,4-diazepane), NS3920 (1-(6-bromopyridin-3-yl)-1,4-diazepane) and (+/-)-epibatidine were prepared at NeuroSearch A/S (Ballerup, Denmark) (Audouze et al., 2006; Peters et al, 1999). Acetylcholine (ACh) (2-acetyloxyethyl(trimethyl)azanium chloride; Sigma-ID A9101), (-)-cytisine ((1S,9S)-3,11-Diazatricyclo[7.3.1.03,8]trideca-5,7-dien-4-one; Sigma-ID C2899), (-)-nicotine ((−)-1-Methyl-2-(3-pyridyl)pyrrolidine (+)-bitartrate; Sigma-ID N5260), and salts or other chemicals not specifically mentioned below were purchased from Sigma (Broenby, Denmark) and were of analytical grade. [^{3}H]Epibatidine (250μCi, (1R,2R,4S)- (+) -6-(6-chloro-3-pyridyl)-7-azabicyclo[2.2.1] heptane PerkinElmer-ID NET1102250UC) was from PerkinElmer (Skovlunde, Denmark). Restriction enzymes, *Sf*9 cells, and pFastBac vector were purchased from Invitrogen (Naerum, Denmark). Oligonucleotides as well as sequencing services were from Eurofins MWG Operon (Ebersberg, Germany).

Mutagenesis, protein expression, and purification- The wild-type (wt) *Ls*-AChBP cDNA was mutated using the overlap extension PCR method (Ho et al., 1989). Briefly, fragments were first primed on the wt sequence to obtain the R104H mutation construct. Then the primers containing both L112Q and M114T mutations were used on the R104H construct to obtain the R104H/L112Q/M114T construct. PCR fragments were digested using EcoRI/BamHI and then purified using agarose gel electrophoresis. Digested inserts were ligated into a cut pFastBac vector. After transformation, each mutant plasmid was purified using a Qiagen miniprep kit. The mutations were then verified by sequencing. Wt and engineered recombinant *Ls*-AChBPs were expressed using the Bac-to-Bac baculovirus expression system in *Sf*9 insect cells and purified using ion exchange and gel filtration chromatography as described previously (Brejc et al., 2001).

6

Cloning of the human α4 and β2 nAChRs and construction of concatenated receptors were described previously (Timmermann et al., 2007). Point mutations to give α4H142V, α4Q150F and α4T152L were introduced by site directed mutagenesis, as previously described (Harpsøe et al., 2011). cRNA was prepared from linearized plasmid using the mMessage mMachine T7 Transcription kit (Invitrogen, Naerum, Denmark) according to manufacturers protocol.

Radioligand binding- Binding experiments with *Ls*-AChBP and *Ls*-AChBP^{HQT} were carried out using the purified protein from *Sf*9 cells under conditions similar to previous descriptions (Harpsøe et al., 2011; Harpsøe et al., 2013). Binding affinity of [^{3}H]epibatidine (K_d) was determined in standard saturation assays where the amount of radioactivity bound after equilibration with protein was measured as a function of the concentration of [^{3}H]epibatidine. Nine volumes of protein suspended in 50 mM Tris-HCl buffer (pH 7.4) were mixed with one volume of [^{3}H]epibatidine (55.8 Ci/mmol, in 48 % ethanol) in varying concentrations and incubated for 2 up to 4 h at room temperature. Nonspecific binding was tested by incubation with an excess of (-)-nicotine (30 µM for wt *Ls*-AChBP and 500 µM for *Ls*-AChBP^{HQT}). Binding was terminated by the addition of ice cold Tris-HCl buffer, and the solution was poured directly onto Whatman GF/C fiberglass filters pre-soaked for 30 min in 0.1 % polyethyleneimine and washed twice with buffer.

Compound inhibition constants (IC$_{50}$'s) were determined in [^{3}H]epibatidine displacement experiments. Eight volumes protein suspension was mixed with one volume of compound solutions in 48 % ethanol and one volume of a [^{3}H]epibatidine solution in 48 % ethanol. Final radioligand concentration was ~1 nM. The specific concentration of the radioligand solution was determined by liquid scintillation counting for each experiment. Nonspecific binding was tested by incubation with (-)-nicotine as described above. Following 1 h incubation at room temperature, binding was terminated by filtration over GF/C fiberglass filters as described above.

Filters containing protein and bound radioligand were individually incubated for at least 4 h with 3 ml Ultima Gold (PerkinElmer). Radioactivity was then measured by conventional liquid scintillation counting on a Tri-Carb counter (PerkinElmer). For each experimental set three measurements were

MOL #98061

performed to determine total and nonspecific binding. All measurements for controls and compound tests were performed as triplicate samples.

Dissociation constant (K_d) values of [^{3}H]epibatidine for each saturation binding experiment was determined by fitting the data by non-linear regression to the equation $Y = (Sb_{max} * x)/(K_d + x)$, where Y equals the specific binding counts (measured binding – measured nonspecific binding), Sb_{max} is the maximal specific binding and x the concentration of radioligand. Average K_d values were calculated from pK_d values. For radioligand displacement experiments compound IC_{50} values were determined by fitting percentage inhibition by nonlinear regression to the equation $Y = 100/(1+10^{X - \log(IC_{50})})$, where Y is the percentage inhibition and X is the logarithm of the compound concentration. Inhibition constant (K_i) values were calculated from IC_{50} values by the Cheng-Prusoff equation $K_i = IC_{50}/(1+L/K_d)$, where L is the concentration of radioligand used in the assay and K_d is the affinity of the radioligand for the binding site under investigation. Average K_i values were calculated from pK_i values. All fitting routines were performed using GraphPad Prism 5.

Two-electrode voltage clamp electrophysiology- Xenopus laevis oocytes were prepared as previously described (Mirza et al., 2008). Briefly, to obtain isolated oocytes, lobes from ovaries of female adult *Xenopus laevis* were removed and defolliculated using collagenase. Oocytes were injected with a total of ~25 ng of a mixture of cRNAs, encoding the nAChR subunits α4, α4H142V, α4Q150F, α4T152L, β2 or concatenated subunits thereof, and incubated for 2-7 days at 18 °C in modified Barth's solution (90 mM NaCl, 1.0 mM KCl, 0.66 mM NaNO₃, 2.4 mM NaHCO₃, 10 mM HEPES, 2.5 mM sodium pyruvate, 0.74 mM CaCl₂, 0.82 mM MgCl₂, 100 µg/ml gentamycin and pH adjusted to 7.5).

Electrophysiological recordings were performed with oocytes placed in a custom-built recording chamber as described previously (Mirza et al., 2008). Pipettes were backfilled with 2 M KCl and open pipette resistances ranged 0.6 - 2.0 MΩ when submerged in OR2 (90 mM NaCl, 2.5 mM KCl, 2.5 mM CaCl₂, 1.0 mM MgCl₂, 5.0 mM HEPES and pH adjusted to 7.5). Cells were voltage clamped at a holding potential ranging from -40 to -80 mV using an Axon Geneclamp 500B amplifier (Molecular Devices, UK). Compounds were dissolved in OR2 on the day of the experiment and solutions were applied to the

8

oocytes with a flow rate of 2.0 ml/min via a glass capillary. Each application lasted ~1 min and the application system ensured rapid solution exchange (in the order of few seconds). Amplified signals were low-pass filtered at 20 Hz and digitized at 200 Hz by an Axon Digidata 1322A (Molecular Devices, UK). Traces were recorded using Clampex 9.2 and analyzed in Clampfit.

During analysis, traces were baseline subtracted and responses to individual applications read as peak current amplitudes. Peak current amplitudes were next normalized to a 1 mM ACh-evoked response in the same oocyte and fitted by nonlinear regression to monophasic or biphasic Hill equations using GraphPad Prism. In the fitting routines, Hill slopes were constrained to 1, the efficacy at infinitely low compound concentrations set to zero and the best fit, mono- *vs.* biphasic, was determined by an F test.

Crystallization- A solution of *Ls*-AChBP^{HQT} in 20 mM Tris-HCl buffer (pH 8.0) and 20 mM NaCl was incubated with 10-25 mM of the ligand (in 20 mM Tris-HCl buffer pH 8.0) prior to crystallization. Crystals of both complexes were obtained using the hanging drop vapor diffusion method at 20°C. Crystallization drops were made by mixing 1 µl of a 5 mg/ml protein:ligand solution with 1 µl of crystallization solution containing 0.1 M Tris-HCl buffer (pH 8.0), 1-3 % v/v polyethylene glycol (PEG) 400, and 1.8-2.3 M $(NH_4)_2SO_4$. Crystals grew from 3 days to 2 weeks to a final length of 0.1-0.2 mm.

Crystallographic data collection, refinement, model building, and structural analysis- The mother liquor supplemented with 25 % (v/v) glycerol was used as cryo-protectant. The crystals were mounted in cryo-loops and flash-cooled in liquid nitrogen after brief immersion in the cryo-protectant solution. X-ray data on the NS3920-*Ls*-AChBP^{HQT} complex were collected on beamline I911-3 at the MAX-lab synchrotron, Lund, Sweden and the data on the NS3573 complex were collected on ID23-2 at the ESRF synchrotron, Grenoble, France, using a marmosaic 225 detector at a wavelength of 1 Å. Data were processed and scaled using *XDS* (Kabsch, 2010) and *Scala* (Leslie, 1992), respectively. Five percent of the data were set aside during the scaling process as test set for calculation of R_{free}.

The structures were solved by the molecular replacement method using the program *Phaser* (McCoy et al., 2007). A pentamer of the *Ls*-AChBP wt complexes with corresponding ligands (pdb ids: 3u8m and 3u8k) was used as search models for the NS3920 and NS3573 complexes, respectively. The refinements

were performed with *Phenix* (Afonine et al., 2012) and rebuilt interactively using *Coot* (Emsley and Cowtan, 2004; Emsley et al., 2010). Non-crystallographic symmetry (NCS) was used during refinement of the NS3920-AChBP^{HQT} complex with *Phenix* as there were eight pentamers in the asymmetric unit of the crystal. The translation-libration-screw (TLS) refinement was also used in the last refinement cycles of NS3920-AChBP^{HQT} structure. The B factors were refined as individual isotropic values. Data collection and refinement statistics are summarized in Table 1.

The quality of the final models was assessed by examination of the detailed stereochemistry using *Molprobity* (Chen et al., 2010) (Table 1). The structure and ligand analyses were performed using *Coot* (Emsley and Cowtan, 2004; Emsley et al., 2010) and *PyMOL* (Schrödinger, New York, NY). The figures were generated using *PyMOL*.

RESULTS

We first mutated the *Ls*-AChBP ligand binding site to make it resemble an α4β2 nAChR α-α interface (*Ls*-AChBP^{HQT}) by introduction of three point mutations, R104H, L112Q, and M114T.

Radioligand binding- To evaluate the *Ls*-AChBP^{HQT} construct as a model system for the α-α interface of α4β2 nAChRs assembled in the 3α:2β stoichiometry and to compare it to the wt *Ls*-AChBP, we initially investigated [^{3}H]epibatidine radioligand binding to the two proteins. For both, [^{3}H]epibatidine displayed saturable specific binding with linear Scatchard plots consistent with a single type of binding sites (higher order fits were not statistically better), albeit the concentration ranges of radioligand used were very different (Fig. 2*A* and 2*B*). The average of determined epibatidine K_d values for the wt *Ls*-AChBP was 0.085 nM (pK_d ± S.D.: 10.1 ± 0.31; n = 3), which is very close to the previously published value of 0.097 nM at a *Ls*-AChBP/5HT$_{3A}$ chimera construct (Rohde et al., 2011). For *Ls*-AChBP^{HQT}, the average K_d value was 16 nM (Table 2), which is approximately 200 fold lower compared to the wt *Ls*-AChBP but very similar to the K_d value of 5.3 nM reported for the functional α4β2^{HQT} mutant receptor (Ahring et al., 2015). When normalized, binding data from all experiments were well approximated by the Hill equation giving EC$_{50}$ values similar to the average of K_d values from the individual experiments (Fig. 2*C*). The

10

figure shows that adequate concentration ranges of [^{3}H]epibatidine have been applied on both wt and engineered Ls-AChBP^{HQT} and that there is good agreement between the EC$_{50}$ values derived for wt and engineered Ls-AChBP^{HQT} and α4β2 and α4β2^{HQT}, respectively. As is also evident from the figure, the curve for the Ls-AChBP^{HQT} is right-shifted by more than two orders of magnitude relative to wt Ls-AChBP, while it quite accurately approximates the affinity measured in the α4β2^{HQT} mutant receptor (Table 2).

Subsequently, a series of agonists were profiled by radioligand displacement studies at Ls-AChBP^{HQT} and compared to data obtained on the α4β2^{HQT} mutant receptor heterologously expressed in HEK293 cells (Ahring et al., 2015). The determined binding affinities for the agonists strictly follow the order obtained on the α4β2^{HQT} receptor as clearly seen from a correlation plot (Fig. 3, Table 2). This underscores that the Ls-AChBP^{HQT} construct is a viable model system that reproduces binding affinities obtained at its functional counterpart.

Crystal structure analysis- Crystal structure analysis was undertaken on complexes between Ls-AChBP^{HQT} and the compounds NS3920 and NS3573 (Fig. 1*B*), which were selected as representatives of ligands that show high and low affinity at the α4β2^{HQT} nAChR, respectively (Table 2) and have distinctly different pharmacological profiles as illustrated in Fig. 1*C*. Both compounds are prototypical nAChR agonists consisting of a pyridine ring connected to a homopiperazine ring that is protonated at physiological conditions. The pyridine ring of NS3920 is substituted with bromine at the 6-position whereas NS3573 has an ethoxy substituent in the pyridine 5-position (Fig. 1*B*). The crystal structures of Ls-AChBP^{HQT} with NS3920 and NS3573 were determined at 2.7 and 2.8 Å resolution and refined to a final R_{work}/R_{free} of 0.19/0.24 and 0.19/0.23, respectively (for information on refinement statistics, see Table 1). The structures show the same homopentameric assembly as previously determined AChBP structures, in which individual monomers consist of an *N*-terminal α-helix, two short α3$_{10}$ helices and a 10-stranded β-sandwich core (Fig. 4). The electron density maps clearly reveal the existence of a single binding orientation for both of the ligands (Fig. 5), whereas the loop F part of the structures (residues

11

154–160) could only be completely modeled in chain D of the NS3573 complex (Fig. 4), due to lack of clear electron density, signifying a greater flexibility of these parts of the protein.

Comparing *Ls*-AChBP^{HQT} complexes with NS3920 and NS3573 to the corresponding wt *Ls*-AChBP complexes (Rohde et al., 2011) shows that neither a significant Cα backbone change (rmsd: 0.258 ± 0.007 Å between the NS3920 complexes and 0.246 ± 0.001 Å between NS3573 complexes) nor ligand repositioning to a different pose occurs (Fig. 5*A* and *B*). Also, the size and shape of the binding site is similar between the wt *Ls*-AChBP and *Ls*-AChBP^{HQT} complexes.

Ligand interactions with non-mutated residues in Ls-AChBP^{HQT} and Ls-AChBP- In the NS3920 structure with *Ls*-AChBP^{HQT}, the core of the ligand (defined as the two conjugated ring systems without substituents) interacts essentially as observed in prototypical agonist-bound structures of AChBP (Celie et al., 2004). The protonated secondary nitrogen of the ligand lies within hydrogen-bonding distance of the backbone carbonyl oxygen of W143, and is also in close contact with the hydroxyl group of Y89 on the principal side of the interface (Fig. 5*A*). On the complementary side, NS3920 interacts with the protein main chain *via* a water-mediated hydrogen bond as previously reported in agonist-bound AChBP structures (Celie et al., 2004; Rohde et al., 2011; Hansen et al., 2005) (Fig. 5*A*). The anchoring of the ligand to the complementary subunit is further supported by a halogen bond interaction caused by the positive electrostatic potential on the tip of the bromine atom of the ligand and electrons in the π-system of the carbonyl oxygen of Q112 (Fig. 5*A,* Br-O distance of 3.1 ± 0.1 Å), similar to the interaction seen in the complex with wt *Ls*-AChBP (Rohde et al., 2011).

The *Ls*-AChBP^{HQT} structure in complex with NS3573 reveals similar interactions between ligand and residues that are unaltered between *Ls*-AChBP^{HQT} and *Ls*-AChBP, both on the principal and the complementary sides of the interface, as observed with the NS3920 (Fig. 5*B*).

Ligand-AChBP^{HQT} specific interactions- Stacking interaction is seen between H104 and the aromatic ring of NS3920 (3.5 ± 0.2 Å averaged over the shortest distance between H104 and the ligand). The ligand stabilizes H104 in a conformation where it forms a hydrogen bond across the interface to Y192 (loop C) on the principal side (Fig. 5*A*). In four out of 40 monomers of the asymmetric unit of the crystal (chains

12

MOL #98061

A, E, Q and b), a water molecule is observed in optimal hydrogen-bonding distance to H104 (2.7 ± 0.1 Å) and two alternate conformations of the histidine (ring flip) have therefore been introduced at these sites. The side-chain amide group of Q112 is in direct contact with the positive edge of the aromatic ring of NS3920 (3.6 ± 0.2 Å) and T114 is within van der Waals interaction distance (3.5 ± 0.2 Å) of the aromatic ring of the ligand (Fig. 6*A*).

In the NS3573 complex, the ethoxy substituent causes a different orientation of H104 and prevents it from interacting across the interface with Y192, causing the loop C to be more open compared to in the NS3920-*Ls*-AChBP^{HQT} complex (7.8 ± 0.05 *vs.* 7.1 ± 0.03 Å measured from the carbonyl oxygen of W143 to the sulfur atom of C187, Fig. 5*C*). This conformation of H104 subsequently leads to a conformational change in its immediate neighbor, Q73. The residue Q73 forms hydrogen bonds across the interface to H146 and E149 on the principal side (Fig. 5*D*). However, as Q73 corresponds to a serine in α4 (S110), we have not found it relevant to further pursue. With regard to conserved residues, the side chain of H104 is within van der Waals distance of the ethoxy substituent of the ligand (3.5 ± 0.1 Å). Likewise, the residues Q112 and T114 are within van der Waals interaction distance of the ethoxy substituent and aromatic ring of the ligand, respectively (Fig. 6*B*).

Mutational analysis- To investigate the functional importance of the three α-α interface "signature" residues in wt α4β2 nAChRs, three point mutated α4 constructs were created. In these, the residues H142, Q150, and T152 on the complementary face of the α(-) subunit were individually mutated to the corresponding β(-) residues, V136, F144, and L146. Hence, each "signature" residue point mutant alters the α-α interface to become more α-β-interface like in one specific position. ACh, NS3920 and NS3573 were then evaluated by two-electrode voltage-clamp electrophysiology on the variant receptors expressed in *Xenopus laevis* oocytes in the 3α:2β stoichiometry. Initial tests with ACh confirmed that all mutants were functional. Next, CRRs for NS3920 and NS3573 were obtained with each construct and compared with data for the wt 3α:2β receptor. For NS3920, the α4H142V mutation resulted in a dramatic right shift of the concentration response curve, rendering the compound approximately 100 fold less potent, whereas the two other mutations had little or no effect on potency (Fig. 7 *A* and *B* and Table 3). In contrast, for

13

MOL #98061

NS3573, the α4H142V mutation had negligible effect whereas both of the other two mutations, α4Q150F

and α4T152L, rendered the compound approximately 10 fold more potent. Interestingly, efficacy levels of

the compounds were also affected but by different residues. For NS3920 a super-agonist response was

observed with the α4Q150F mutant whereas for NS3573, the efficacy was more than doubled with both

α4Q150F and α4T152L relative to wt α4β2 nAChR (Fig. 7 *B* and Table 3).

DISCUSSION

The binding and functional differences observed at 3α:2β and 2α:3β nAChRs are assigned to existence of

a third ACh binding site at the α-α interface of α4β2 receptors with 3α:2β stoichiometry and more

specifically to the three "signature" residues at the complementary side of this interface. To resolve the

structural determinants leading to differential agonist characteristics at α-α and α-β binding sites, *Ls*-

AChBP was engineered to resemble the α-α interface of 3α:2β nAChRs. The construct, *Ls*-AChBP^{HQT},

reproduces binding affinities of the α4β2^{HQT} receptor with high accuracy for a series of agonists with an

affinity range spanning from nano- to micromolar (Fig. 3). The high degree of ligand affinity correlation

between *Ls*-AChBP^{HQT} and α4β2^{HQT} receptors suggest that detailed structural information regarding

ligand binding at the α-α interface can be obtained from co-crystal structures with *Ls*-AChBP^{HQT}.

Therefore, we used *Ls*-AChBP^{HQT} to investigate interactions for two agonists, NS3920 and NS3573. From

co-crystal structures and functional studies we show that residues specific to the α-α interface play

differential roles in determining binding affinities of the ligands, of which the ligand-specific role of

α4H142 is particularly pronounced.

NS3920 and NS3573 are both homopiperazine substituted pyridines and have comparable binding affinity

and functional potency at 2α:3β receptors (Rohde et al., 2011). However, the pharmacological properties

of NS3920 and NS3573 differ significantly at 3α:2β receptors with respect to both binding affinities and

functional electrophysiological profiles. NS3920 has approximately 70 fold higher affinity compared to

NS3573 at the α4β2^{HQT} receptor (Table 2) and is virtually a full agonist at the wt 3α:2β receptor with a

monophasic CRR, suggesting that it does not differentiate between the α-β and α-α sites to a notable

extent (Fig. 1*C*). In contrast, NS3573 is a partial agonist with a biphasic CRR at 3α:2β receptors, displaying an almost 1000 fold potency difference between α-β and α-α sites (Fig. 1*C*) (Harpsøe et al., 2011; Ahring et al., 2015). NS3920 and NS3573 therefore represent two compounds that are particularly suitable for studying differences in interactions with α-α and α-β interfaces of 3α:2β receptors.

The most striking difference between the co-crystal structures of *Ls*-AChBP^{HQT} with NS3920 and NS3573 is the different rotameric states of H104. In the *Ls*-AChBP^{HQT} complex with NS3920, H104 stacks with the aromatic ring of the ligand (Fig. 6*A*) whereas in the complex with NS3573, H104 adopts an entirely different orientation, which is comparable to that of R104 in wt *Ls*-AChBP. In the observed binding mode for NS3920, H104 forms a hydrogen bond to Y192 on loop C. Effectively; this is an inter-subunit bridge that mediates contacts between principal and complementary subunits in this structure and reinforces the ligand-mediated contacts. At the same time, this interaction constrains loop C to be more closed relative to the structure in complex with NS3573 (Fig. 5*C*). In the NS3573 complex, H104 makes favorable van der Waals contacts to the ethoxy substituent and at the same time causes a displacement of Q112 to a position where it interacts with the ethoxy substituent of the ligand (3.5 ± 0.2 Å) (Fig. 5*D*). The consequences of the Q112 displacement in terms of binding affinity are unclear. The combination of no halogen bonding (Rohde et al., 2011), the lack of stacking interactions with H104 and no inter-subunit bridge formation to Y192 in the NS3573 complex likely account for the decreased affinity of NS3573 relative to NS3920 at the *Ls*-AChBP^{HQT} and α4β2^{HQT} receptors.

The different positions of H104 in the two co-crystal structures is supported by the mutational data showing that mutation of α4H142 to a valine, which is the corresponding residue in the β2 subunit, has entirely different effects on the pharmacology of NS3920 and NS3573 at receptors expressed in the 3α:2β stoichiometry. For NS3920 efficacy is decreased from 82 to 54 % accompanied by a dramatic ~50 fold loss of functional potency (Table 3). This suggests that for NS3920, H142 is important not only for binding but also contributes to gating of the receptor. For NS3573, where the histidine is pointing away from the binding site, mutation of H142 to valine showed only marginal effects on efficacy and potency and did not change the fundamental appearance of the CRR (Fig. 7*B*). We have previously suggested that

15

inter-subunit bridge formation rather than the closure of loop C is the important determinant of efficacy (Rohde et al., 2011; Harpsøe et al., 2013). The high efficacy of NS3920 along with the strong effect observed upon mutation of the histidine and the breakage of its hydrogen bond to Y192 further support this hypothesis.

Interestingly, mutation of the two remaining "signature" residues Q150 and T152 to their β2 counterparts, phenylalanine and leucine, respectively, has little effect on the functional potency of NS3920. For NS3573 on the other hand, the mutations each resulted in ~10 fold increase in potency towards that of the 2α:3β receptor (Table 3, Fig. 7). This signifies an important contribution of each of these residues in discriminating binding affinities between α-α and α-β binding sites. For NS3920, the dominant role of H142 along with the very small difference in binding affinity (approximately 10 fold) between α-α and α-β sites leave little room for improvement by mutation and it is therefore not surprising that no differences are observed by mutation of these residues.

The important observation from the mutational studies is that each residue plays a unique role in interaction with different ligands. For some residues, the effect appears mainly on binding affinity while for others, efficacies are also affected. For both compounds, the Q150F mutant increases efficacy to roughly twice that at the wt receptor and NS3920 is essentially a super-agonist. For NS3920 the T152L mutant lowers efficacy, whereas it increases efficacy of NS3573. The differential role of the "signature" residues is thus fully in line with the studies showing that the complementary face of the adjacent subunit plays a key role fine-tuning agonist function (Harpsøe et al., 2013; Marotta et al., 2014).

Interestingly, despite an overall conserved positioning of the ligands in the pocket, the interactions with the three "signature" residues is entirely different between *Ls*-AChBP^{HQT} and its wt variant (compare Fig. 6*A*/*C* and 6*B*/*D*). The difference is reflected in a consistently higher affinity of the compounds in Table 2 at wt *Ls*-AChBP in agreement with an expected stronger interaction of lipophilic compounds with a hydrophobic binding site. In the *Ls*-AChBP^{HQT} binding site, the presence of H104, Q112, and Thr114 creates a more hydrophilic environment, which generally, unless specific interactions can be obtained, leads to lower affinity for CNS-type compounds.

16

In combination, wt *Ls*-AChBP and *Ls*-AChBP^{HQT} structures may facilitate understanding of the stoichiometry selectivity of agonists, such as sazetidine-A (Xiao et al., 2006), which is an agonist with a functional preference for 2α:3β receptors (Zwart et al., 2008). In a recent study, it has been suggested that sazetidine-A is excluded from binding at the α-α interface because of steric clashes with α4H142 (Mazzaferro et al., 2014). However, if this was the case, it could be expected that NS3573, which, like sazetidine-A, contains a large substituent in the pyridine 5-position, would be affected in a similar way. Our data indicate that the 5-substituent induced conformational change of His142 to an un-favorable rotameric state leads to a large drop in affinity and functional potency as well as efficacy of the ligand but not its exclusion from binding *per se*.

In the present study, we adopted a minimalistic approach and only mutated residues in immediate vicinity of the agonist binding pocket in *Ls*-AChBP. A big advantage with this approach was that expression, purification and crystallization conditions could be adapted from the conditions used with the wt protein without the need for time-consuming optimization of the process. The approach led to a construct that in terms of binding affinities correlates almost perfectly with binding affinities obtained in the functional α4β2^{HQT} receptor for agonists (Fig. 3). The minimalistic mutational approach means that the binding pocket is engineered to recognize agonists. For antagonists that usually are larger structures and extend out of the agonist binding core, an equally good correlation cannot automatically be assumed. To accommodate such ligands a more comprehensive mutational approach could be adopted. This has been successfully done for the nAChR α7 in a chimeric construct with *Ac*-AChBP that was shown to accommodate both agonists and antagonists (Li et al., 2011; Nemecz and Taylor, 2011).

The interpretation of binding and function in a structural context requires a unique well-defined response. For receptors with 3α:2β stoichiometry the present and previous studies (Rohde et al., 2011; Ahring et al., 2015) have taught us that binding and function correlates for nAChRs if focusing on a response that can be mapped back to one individual type of binding sites. In these instances binding and function can be interpreted in a structural context. This study shows that to investigate structure activity relationships

17

superior correlation between an engineered *Ls*-AChBP and its functional counterpart can be obtained with a minimalistic mutation approach.

Targeting binding sites at non α-β interfaces of nAChRs provides a unique opportunity to develop subtype or even stoichiometry selective therapeutics. To aid structure based design of such ligands, engineered AChBPs may be used as structural models and can provide details about ligand receptor interactions that by far exceeds what can be obtained using wt AChBPs as models.

Authorship Contributions:

Participated in research design: Shahsavar, Ahring, Olsen, Kastrup, Balle and Gajhede

Conducted experiments: Shahsavar, Ahring, Olsen and Krintel

Performed data analysis: Shahsavar, Ahring, Olsen, Kastrup, Balle and Gajhede

Wrote the first draft of the manuscript: Shahsavar and Gajhede

REFERENCES

Afonine PV, Grosse-Kunstleve RW, Echols N, Headd JJ, Moriarty NW, Mustyakimov M, Terwilliger TC, Urzhumtsev A, Zwart PH and Adams PD (2012) Towards automated crystallographic structure refinement with phenix.refine. *Acta. Crystallogr. D. Biol. Crystallogr.* **68**: 352-367.

Ahring PK, Olsen JA, Nielsen EØ, Peters D, Pedersen MHF, Rohde LA, Kastrup JS, Shahsavar A, Indurthi D, Chebib M, Gajhede M and Balle T (2015) Engineered a4b2 Nicotinic Acetylcholine Receptors as Models for Measuring Agonist Binding and Effect at the Orthosteric Low-affinity a4-a4 Interface. *Neuropharmacology* doi: 10.1016/j.neuropharm.2014.12.035.

Althoff T, Hibbs RE, Banerjee S and Gouaux E. (2014) X-ray structures of GluCl in apo states reveal a gating mechanism of Cys-loop receptors. *Nature* **512**: 333-337.

Audouze K, Nielsen EØ, Olsen GM, Ahring PK, Jørgensen TD, Peters D, Liljefors T and Balle T (2006) New Ligands with Affinity for the alpha4beta2 Subtype of Nicotinic Acetylcholine Receptors. Synthesis, Receptor Binding, and 3D-QSAR Modeling. *J. Med. Chem.* **49**: 3159-3171.

Bocquet N, Nury H, Baaden M, Le Poupon C, Changeux J-P, Delarue M and Corringer P-J (2009) X-ray structure of a pentameric ligand-gated ion channel in an apparently open conformation. *Nature* **457**: 111-114.

Brejc K, van Dijk WJ, Klaassen RV, Schuurmans M, van Der Oost J, Smit AB and Sixma TK (2001) Crystal structure of an ACh-binding protein reveals the ligand-binding domain of nicotinic receptors. *Nature* **411**: 269-276.

Carbone AL, Moroni M, Groot-Kormelink PJ and Bermudez I (2009) Pentameric concatenated $(a4)_2(b2)_3$ and $(a4)_3(b2)_2$ nicotinic acetylcholine receptors: subunit arrangement determines functional expression. *Br. J. Pharmacol.* **156**: 970-981.

Celie PHN, Kasheverov IE, Mordvintsev DY, Hogg RC, van Nierop P, van Elk R, van Rossum-Fikkert SE, Zhmak MN, Bertrand D, Tsetlin V, Sixma TK and Smit AB (2005) Crystal structure of nicotinic acetylcholine receptor homolog AChBP in complex with an alpha-conotoxin PnIA variant. *Nat. Struct. Mol. Biol.* **12**: 582-588.

Celie PHN, van Rossum-Fikkert SE, van Dijk WJ, Brejc K, Smit AB and Sixma TK (2004) Nicotine and carbamylcholine binding to nicotinic acetylcholine receptors as studied in AChBP crystal structures. *Neuron* **41**: 907-914.

Chen VB, Arendall WB 3rd, Headd JJ, Keedy DA, Immormino RM, Kapral GJ, Murray LW, Richardson JS and Richardson DC (2010) MolProbity: all-atom structure validation for macromolecular crystallography. *Acta. Crystallogr. D. Biol. Crystallogr.* **66**: 12-21.

Emsley P and Cowtan K (2004) Coot: model-building tools for molecular graphics. *Acta. Crystallogr. D. Biol. Crystallogr.* **60**: 2126-2132.

Emsley P, Lohkamp B, Scott WG and Cowtan K (2010) Features and Development of Coot. *Acta. Crystallogr. D. Biol. Crystallogr.* **66**: 486-501.

Hansen SB, Sulzenbacher G, Huxford T, Marchot P, Taylor P and Bourne Y (2005) Structures of Aplysia AChBP complexes with nicotinic agonists and antagonists reveal distinctive binding interfaces and conformations. *EMBO J.* **24**: 3635-3646.

Harpsøe K, Ahring PK, Christensen JK, Jensen ML, Peters D and Balle T (2011) Unraveling the High- and Low-Sensitivity Agonist Responses of Nicotinic Acetylcholine Receptors. *J. Neurosci.* **31**: 10759-10766.

Harpsøe K, Hald H, Timmermann DB, Jensen ML, Dyhring T, Nielsen EØ, Peters D, Balle T, Gajhede M, Kastrup JS and Ahring PK (2013) Molecular determinants of subtype-selective efficacies of cytisine and the novel compound NS3861 at heteromeric nicotinic acetylcholine receptors. *J. Biol. Chem.* **288**: 2559-2570.

Hassaine G, Deluz C, Grasso L, Wyss R, Tol MB, Hovius R, Graff A, Stahlberg H, Tomizaki T, Desmyter A, Moreau C, Li X-D, Poitevin F, Vogel H and Nury H (2014) X-ray structure of the mouse serotonin 5-HT3 receptor. *Nature* **512**: 276-281.

Hibbs RE and Gouaux E (2011) Principles of activation and permeation in an anion-selective Cys-loop receptor. *Nature* **474**: 54-60.

Hilf RJ and Dutzler R (2008) X-ray structure of a prokaryotic pentameric ligand-gated ion channel. *Nature* **452**: 375-379.

Hilf RJ and Dutzler R (2009) Structure of a potentially open state of a proton-activated pentameric ligand-gated ion channel. *Nature* **457**: 115-118.

Ho SN, Hunt HD, Horton RM, Pullen JK and Pease LR (1989) Site-directed mutagenesis by overlap extension using the polymerase chain reaction. *Gene* **77**: 51-59.

Jensen AA, Frølund B, Liljefors T and Krogsgaard-Larsen P (2005) Neuronal nicotinic acetylcholine receptors: structural revelations, target identifications, and therapeutic inspirations. *J. Med. Chem.* **48**: 4705-4745.

Kabsch W (2010) XDS. *Acta. Crystallogr. D. Biol. Crystallogr.* **66**: 125-132.

Kuryatov A, Luo J, Cooper J and Lindstrom J (2005) Nicotine acts as pharmacological chaperone to up-regulate human a4b2 acetylcholine receptors *Mol. Pharmacol.* **68**: 1839-1851.

Leslie AGW (1992) Joint CCP4 + ESF-EAMCB Newsletter on Protein Crystallography. **26**.

Li S-X, Huang S, Bren N, Noridomi K, Dellisanti CD, Sine SM and Chen L (2011) Ligand-binding domain of an [alpha]7-nicotinic receptor chimera and its complex with agonist. *Nat. Neurosci.* **14**: 1253-1259.

Marotta CB, Rreza I, Lester HA and Dougherty DA (2014) Selective ligand behaviors provide new insights into agonist activation of nicotinic acetylcholine receptors. *ACS Chem. Biol.* cb400937d.

Mazzaferro S, Gasparri F, New K, Alcaino C, Faundez M, Iturriaga Vasquez P, Vijayan R, Biggin PC and Bermudaz I (2014) Non-equivalent ligand selectivity of agonist sites in (a4b2)2a4 nicotinic acetylcholine receptors: a key determinant of agonist efficacy. *J. Biol. Chem.* **289**: 21795-21806.

McCoy AJ, Grosse-Kunstleve RW, Adams PD, Winn MD, Storoni LC and Read RJ (2007) Phaser crystallographic software. *J. Appl. Crystallogr.* **40**: 658-674.

Miller PS and Aricescu AR (2014) Crystal structure of a human GABAA receptor. *Nature* **512**: 270-275.

Mirza NR, Larsen JS, Mathiasen C, Jacobsen TA, Munro G, Erichsen HK, Nielsen AN, Troelsen KB, Nielsen EØ and Ahring PK (2008) NS11394 [3'-[5-(1-hydroxy-1-methyl-ethyl)-benzoimidazol-1-yl]-biphenyl-2-carbonitrile], a unique subtype-selective GABAA receptor positive allosteric modulator: in vitro actions, pharmacokinetic properties and in vivo anxiolytic efficacy. *J. Pharmacol. Exp. Ther.* **327**: 954-968.

Moroni M, Vijayan R, Carbone A, Zwart R, Biggin PC and Bermudez I (2008) Non-agonist-binding subunit interfaces confer distinct functional signatures to the alternate stoichiometries of the a4b2 nicotinic receptor: an a4-a4 interface is required for Zn+2 potentiation. *J. Neurosci.* **28**: 6884-6894.

Moroni M, Zwart R, Sher E, Cassels BK and Bermudez I (2006) a4b2 nicotinic receptors with high and low acetylcholine sensitivity: pharmacology, stoichiometry, and sensitivity to long-term exposure to nicotine. *Mol. Pharmacol.* **70**: 755-768.

Nelson ME, Kuryatov A, Choi CH, Zhou Y and Lindstrom J (2003) Alternate stochiometries of a4b2 nicotinic acetylcholine receptors. *Mol. Pharmacol.* **63**: 332-341.

Nemecz À and Taylor PW (2011) Creating an a7 nicotinic acetylcholine recognition domain from the acetylcholine binding protein: crystallographic and ligand selectivity analyses. *J. Biol. Chem.* **286**: 42555-42565.

Olsen JA, Ahring PK, Kastrup JS, Gajhede M and Balle T (2014a) Structural and Functional Studies of the Modulator NS9283 Reveal Agonist-Like Mechanism of Action at a4b2 Nicotinic Acetylcholine Receptors. *J. Biol. Chem.* **289**: 24911-24921.

Olsen JA, Balle T, Gajhede M, Ahring PK and Kastrup JS (2014b) Molecular Recognition of the Neurotransmitter Acetylcholine by an Acetylcholine Binding Protein Reveals Determinants of Binding to Nicotinic Acetylcholine Receptors. *PLoS ONE* **9**: e91232.

Peters D, Olsen G, Nielsen EØ and Nielsen SF (1999) Heteroaryl diazabicycloalkanes as cholinergic ligands at nicotinic acetylcholine receptors. WO9921834, NeuroSearch A/S, Ballerup, Denmark.

Rohde LA, Ahring PK, Jensen ML, Nielsen EØ, Peters D, Helgstrand C, Krintel C, Harpsøe K, Gajhede M, Kastrup JS and Balle T (2011) Inter-subunit bridge formation governs agonist efficacy at nicotinic acetylcholine alpha4beta2 receptors; a unique role of halogen bonding revealed. *J. Biol. Chem.* **287**: 4248-4259.

Sauguet L, Shahsavar A, Poitevin F, Huon C, Menny A, Nemecz À, Haouz A, Changeux J-P, Corringer P-J and Delarue M (2013) Crystal structures of a pentameric ligand-gated ion channel provide a mechanism for activation. *Proc. Natl. Acad. Sci. U S A* **111**: 966-971.

Shahsavar A, Kastrup JS, Nielsen EØ, Kristensen JL, Gajhede M and Balle T (2012) Crystal Structure of Lymnaea stagnalis AChBP Complexed with the Potent nAChR Antagonist DHbE Suggests a Unique Mode of Antagonism. *PLoS ONE* **7**: e40757.

Taly A, Corringer P-J, Guedin D, Lestage P and Changeux J-P (2009) Nicotinic receptors: allosteric transitions and therapeutic targets in the nervous system. *Nat. Rev. Drug Discov.* **8**: 733-750.

Tapia L, Kuryatov A and Lindstrom J (2007) Ca+2 permeability of the (a4)3(b2)2 stoichiometry greatly exceeds that of (a4)2(b2)3 human acetylcholine receptors. *Mol. Pharmacol.* **71**: 769-776.

Timmermann DB, Grønlien JH, Kohlhaas KL, Nielsen EØ, Dam E, Jørgensen TD, Ahring PK, Peters D, Holst D, Christensen JK, Malysz J, Briggs CA, Gopalakrishnan M and Olsen GM (2007) An allosteric modulator of the alpha7 nicotinic acetylcholine receptor possessing cognition-enhancing properties in vivo. *J. Pharmacol. Exp. Ther.* **323**: 294-307.

Ussing CA, Hansen CP, Petersen JG, Jensen AA, Rohde LA, Ahring PK, Nielsen EØ, Kastrup JS, Gajhede M, Frølund B and Balle T (2013) Synthesis, pharmacology, and biostructural characterization of novel a4b2 nicotinic acetylcholine receptor agonists. *J. Med. Chem.* **56**: 940-951.

Xiao Y, Fan H, Musachio JL, Wei ZL, Chellappan SK, Kozikowski AP and Kellar KJ (2006) Sazetidine-A, a novel ligand that desensitizes a4b2 nicotinic acetylcholine receptors without activating them. *Mol. Pharmacol.* **70**: 1454-1460.

Zwart R, Carbone AL, Moroni M, Bermudez I, Mogg AJ, Folly EA, Broad LM, Williams AC, Zhang D, Ding C, Heinz BA and Sher E (2008) Sazetidine-A is a potent and selective agonist at native and recombinant a4b2 nicotinic acetylcholine receptors. *Mol. Pharmacol.* **73**: 1838-1843.

FOOTNOTES

FIGURE LEGENDS

Figure 1. Agonist binding sites at α4β2 nAChRs. (A) Schematic representations showing subunit arrangement and interfaces of the $(\alpha4)_2(\beta2)_3$ (left panel) and $(\alpha4)_3(\beta2)_2$ (right panel) ligand binding domains. The high-affinity (α-β) orthosteric agonist binding sites are shown by black arrows and the low-affinity orthosteric binding site at the α-α interface is shown by a grey arrow. The (+) and (-) signs represent the principal and complementary sides of the interface, respectively. (B) Chemical structure of NS3920 in the right panel, and NS3573 in the left panel. (C) Concentration-response curves for NS3920 and NS3573 on $(\alpha4)_2(\beta2)_3$ and $(\alpha4)_3(\beta2)_2$ receptors expressed in *Xenopus laevis* oocytes. Thin hashed lines represent fitted curve extensions. Data are from Harpsøe et al., 2011 (NS3573) and Ahring et al., 2015 (NS3920).

Figure 2. [³H]Epibatidine saturation binding at wt and engineered *Ls*-AChBP^HQT. Protein purified from *Sf*9 cells was used in standard filtration binding assays. (A, B) For both *Ls*-AChBP and *Ls*-AChBP^HQT, normalized specific binding plotted as a function of the [³H]epibatidine concentration was well approximated by a single site hyperbolic model using nonlinear regression. This indicates binding to a single saturable binding site in each case. Plotted datapoints are from n = 3 (*Ls*-AChBP) or n = 4 (*Ls*-AChBP^HQT) independent experiments, with each datapoint representing the mean of a triplicate determination. Note that two of the four curves are overlapping for AChBP^HQT. Individual K_d values derived from fitting are indicated in the graphs and the average K_d values (calculated from pK_d values) were 0.085 nM (pK_d ± S.D. = 10.07 ± 0.31; n = 3) for *Ls*-AChBP and 16 nM (pK_d ± S.D. = 7.80 ± 0.30; n = 4) for *Ls*-AChBP^HQT. At the highest tested [³H]epibatidine concentrations, non-specific binding (mean ± S.D.) equated 12 ± 9 % and 25 ± 12 % of total binding for *Ls*-AChBP and *Ls*-AChBP^HQT, respectively. (C) Normalized specific binding plotted as a function of the logarithm of [³H]epibatidine concentrations were well approximated by the monophasic Hill equation using nonlinear regression. In the presented fits bottom was set to 0 and the Hill slope to 1. Data for wt α4β2 and α4β2^HQT are from Ahring et al., 2015.

Figure 3. Correlation between affinity of nAChR agonists at the engineered *Ls*-AChBP^{HQT} and α4β2^{HQT} nAChR. Linear correlation of pK$_i$ values for a series of agonists at *Ls*-AChBP^{HQT} *vs.* α4β2^{HQT}. Data are presented in Table 2. Dotted lines indicate 95 % confidence intervals. Nic, cyt, and epi stand for nicotine, cytisine and epibatidine, respectively.

Figure 4. Overall structure of *Ls*-AChBP^{HQT}. Cartoon diagram showing homopentameric *Ls*-AChBP^{HQT} on left and the ligand-binding pocket at the interface of two monomers formed by loops A, B, and C from the principal or (+) side (colored in red) and loops D, E, and F from the complementary (-) side (colored in green) on right are presented.

Figure 5. Co-crystal structures of *Ls*-AChBP^{HQT} with NS3920 and NS3573. A magnified view of the ligand binding site at the interface of two monomers in (A) NS3920 and (B) NS3573 complexes with *Ls*-AChBP^{HQT} is shown. The (+) and (-) signs represent the principal and complementary sides of the interface, respectively. The principal side is colored in deep teal and complementary side in pink in NS3920-*Ls*-AChBP^{HQT} complex. NS3573-*Ls*-AChBP^{HQT}, the principal and complementary sides are colored in red and green, respectively. The interactions between the ligand and its surroundings are shown as dashed lines. The final 2mFo-DFc electron density maps at 1σ level carved around the ligands are also presented. (C) Cartoon representation of loop C in the NS3920 (deep teal) and NS3573 (red) complexes with *Ls*-AChBP^{HQT}. (D) The complementary monomer of *Ls*-AChBP^{HQT} crystal structure in complex with NS3920 (pink) is superimposed on the complementary monomer of the *Ls*-AChBP^{HQT} in complex with NS3573 (green). The principal monomers of NS3920 and NS3573 complexes with *Ls*-AChBP^{HQT} are shown in deep teal and red, respectively. The hydrogen-bonding interactions are shown as dashed lines.

Figure 6. The ligand interactions with residues H/R104, Q/L112, and T/M114 in engineered/wt *Ls*-AChBP. (A) NS3920-*Ls*-AChBP^{HQT}, (B) NS3573-*Ls*-AChBP^{HQT}, (C) NS3920-wt *Ls*-AChBP, and (D) NS3573-wt *Ls*-AChBP. The (+) and (-) signs represent the principal and complementary sides of the interface, respectively. The atoms involved in van der Waals interaction are labeled. The sphere in the middle of the aromatic ring of NS3920 in panel (A) represents the centroid of this group. The average distances between the atoms of the protein and the ligands, which are involved in van der Waals interactions are as follows: (A) imidazole ring of His104 and center of the aromatic ring of NS3920: 3.5 ± 0.2 Å, Oε1 of

Q112 and C4 of the aromatic ring of NS3920: 3.5 ± 0.1 Å, Cβ of T114 and N1 of the aromatic ring of NS3920: 3.6 ± 0.2 Å,

(B) Cβ and Cγ of His104 and O1 of the ethoxy substituent of NS3573: 3.5 ± 0.1 Å, Oε1 of Q112 and O1 of the ethoxy

substituent of NS3573: 3.5 ± 0.2 Å, Cβ of T114 and N3 and C10 of the aromatic ring of NS3573: 3.6 ± 0.1 Å, (C) Cβ of R104

and Br of NS3920: 3.4 ± 0.1 Å, Cδ2 of Leu112 and C4 and C5 of NS3920: 3.4 ± 0.1 Å, Cε of M114 and C1, C2 and N2 of

NS3920: 3.4 ± 0.1 Å, (D) Cβ of R104 and O1 of the ethoxy substituent of NS3573: 3.5 ± 0.1 Å, Cδ2 of Leu112 and C7, C12

and O1 of the ethoxy substituent of NS3573: 3.7 ± 0.1 Å, Cε of M114 and C4, N2, C9 and C10 of NS3573: 3.7 ± 0.1 Å.

Figure 7. Agonist-evoked responses at mutant α4β2 nAChRs using *Xenopus laevis* oocyte two-electrode voltage-clamp electrophysiology. To yield uniform populations of receptors in the 3α:2β stoichiometry, oocytes were injected with wt β2 subunits mixed with point mutated α4 subunits in a 4:1 cRNA ratio (red, purple and green curves). Full CRRs were obtained on each oocyte. Peak current amplitudes were background subtracted and normalized to the amplitude evoked by 1 mM ACh (ACh_control) on the same oocyte. Calculated percentage activation were depicted as mean ± S.E. as a function of the concentration and fitted to a mono- or biphasic Hill equation using non-linear regression with a fixed bottom of 0 and Hill slope(s) of 1 (A, B) NS3920 and NS3573 from n = 6-19 individual oocytes. Note the different scaling used for the ordinate axis. Thin hashed lines represent fitted curve extensions. Regression results are presented in Table 3. Data for $(α4)_2(β2)_3$ and $(α4)_3(β2)_2$ with NS3920 are from Ahring et al., 2015 and with NS3573 from Harpsøe et al., 2011.

MOL #98061

TABLES

Table 1. Data collection and refinement statistics.

	NS3920/*Ls*-AChBP^{HQT}	NS3573/*Ls*-AChBP^{HQT}
Data collection		
X-ray source	Synchrotron radiation	Synchrotron radiation
Wavelength (Å)	1.0	1.0
Space group	P2$_1$	P2$_1$2$_1$2
No. of monomers in the asymmetric unit	40	5
Unit cell dimensions		
a, b, c (Å)	135.49, 145.42, 234.91	77.33, 123.10, 127.45
α, β, γ (°)	90.00, 101.29, 90.00	90.00, 90.00, 90.00
Resolution range (Å)	30.07-2.70 (2.85-2.70)^a	49.18-2.83 (2.98-2.83)
R$_{merge}$	0.081 (0.481)	0.212 (1.371)
<I/σI>	15.6 (2.9)	10.5 (2.0)
Completeness (%)	99.4 (96.4)	100 (100)
Multiplicity	3.8 (3.7)	7.8 (7.9)
Overall no. of reflections	921506 (126548)	230838 (33859)
No. of unique reflections	242584 (34273)	29761 (4276)
Wilson B (Å^2)	40.2	38.5
Refinement		
R_{work}/R_{free} (%)	19.8/24.4	19.3/23.1
No. of residues	7955	1004
No. of waters	1052	116
No. of ligands	40	5
Average B-factors (Å^2)		
Protein chains	46	35
Water	30	25
Ligand	44	31
Root mean square deviations		
Bond lengths (Å)	0.01	0.01
Bond angles (°)	1.1	1.1
Ramachandran outliers (%)	0	0
Ramachandran favoured (%)	98.6	97.4
Rotamer outlier (%)	1.3	2.0
C$^\beta$ outlier (%)	2	0
Clash score	3.8	2.9

^{a} Numbers in parentheses represent the last shell values.

Table 2. Binding affinities of nAChR ligands at *Ls*-AChBP^{HQT} and α4β2^{HQT}. *Ls*-AChBP^{HQT} protein was purified from *Sf*9 cells and used in standard filtration binding assays. The pK$_d$ value of [^{3}H]epibatidine was obtained as described in the legend to Fig. 2. Binding affinities represented as pK$_i$ of the remaining compounds were determined as the potency for displacing a fixed concentration of [^{3}H]epibatidine. pK$_i$ values are presented as mean ± S.D. for n = 3-4 determinations each conducted in triplicates. K$_d$ (epibatidine) and K$_i$ values are calculated from pK$_d$ and pK$_i$ values and presented as mean in nM. All data for α4β2^{HQT} are from Ahring et al., 2015.

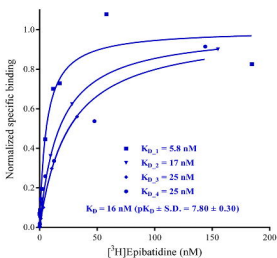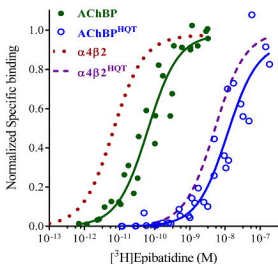|	*Ls*-AChBP^{HQT}		α4β2^{HQT}	
	K$_i$	pK$_i$ ± S.D.	K$_i$	pK$_i$ ± S.D.
	nM		*nM*	
ACh	18000	4.7 ± 0.24	8400	5.1 ± 0.33
Cytisine	580	6.2 ± 0.49	210	6.7 ± 0.34
Epibatidine (K$_d$)	16	7.8 ± 0.30	5.4	8.3 ± 0.12
Nicotine	2200	5.7 ± 0.03	1600	5.8 ± 0.22
NS3531	570	6.2 ± 0.16	190	6.7 ± 0.20
NS3573	1700	5.8 ± 0.14	960	6.0 ± 0.20
NS3920	29	7.5 ± 0.12	13	7.8 ± 0.14

MOL #98061

Table 3. Agonist-evoked responses at wt and mutant α4β2 nAChRs using *Xenopus laevis* oocyte two-electrode voltage-clamp electrophysiology. Data were obtained as described in the legend for Fig. 7. Background subtracted and normalized peak current amplitudes were fitted to a mono- or biphasic Hill equation using non-linear regression with a fixed bottom of 0 and Hill slope(s) of 1 and are presented as EC_{50} in µM (pEC_{50} ± S.E.) and maximal efficacy E_{max} ± S.E. in % of ACh_control (1 mM ACh). "na" indicates not applicable (monophasic fit). Data for $(\alpha4)_2(\beta2)_3$ and $(\alpha4)_3(\beta2)_2$ are from Ahring et al., 2015.

	ACh			NS3573			NS3920	
	EC_{50_1} (pEC_{50_1})	EC_{50_2} (pEC_{50_2})	E_{max}	EC_{50_1} (pEC_{50_1})	EC_{50_2} (pEC_{50_2})	E_{max}	EC_{50} (pEC_{50})	E_{max}
	µM	*µM*	*%*	*µM*	*µM*	*%*	*µM*	*%*
$(\alpha4)_2(\beta2)_3$	1.3 (5.9 ± 0.025)	na	100 ± 1.1	0.020 (7.7 ± 0.051)	na	41 ± 1.0	0.056 (7.2 ± 0.034)	62 ± 1.2
$(\alpha4)_3(\beta2)_2$	1.3 (5.9 ± 0.19)	130 (3.9 ± 0.066)	98 ± 1.8	0.0089 (8.1 ± 0.36)	8.5 (5.1 ± 0.21)	23 ± 1.7	0.053 (7.3 ± 0.054)	82 ± 2.0
$(\alpha4^{H142V})_3(\beta2)_2$	10 (5.0 ± 0.13)	400 (3.4 ± 0.14)	100 ± 2.6	0.016 (7.8 ± 0.57)	7.9 (5.1 ± 0.13)	40 ± 3.2	2.8 (5.6 ± 0.063)	54 ± 3.0
$(\alpha4^{Q150F})_3(\beta2)_2$	0.8 (6.1 ± 0.25)	200 (3.7 ± 0.073)	98 ± 2.7	0.016 (7.8 ± 0.46)	1.6 (5.8 ± 0.16)	66 ± 3.1	0.12 (6.9 ± 0.081)	125 ± 5.6
$(\alpha4^{T152L})_3(\beta2)_2$	3.2 (5.5 ± 0.068)	130 (3.9 ± 0.12)	100 ± 1.3	0.29 (6.5 ± 0.059)	na	58 ± 1.6	0.049 (7.3 ± 0.071)	57 ± 2.4

30

Figure 1

A

Ls-AChBP

- $K_{D\_1} = 0.099$ nM
- $K_{D\_2} = 0.16$ nM
- $K_{D\_3} = 0.039$ nM

$K_D = 0.085$ nM ($pK_D \pm$ S.D. $= 10.07 \pm 0.31$)

B

Ls-AChBP^{HQT}

- $K_{D\_1} = 5.8$ nM
- $K_{D\_2} = 17$ nM
- $K_{D\_3} = 25$ nM
- $K_{D\_4} = 25$ nM

$K_D = 16$ nM ($pK_D \pm$ S.D. $= 7.80 \pm 0.30$)

C
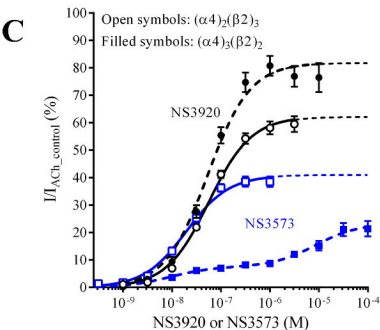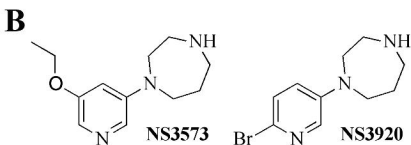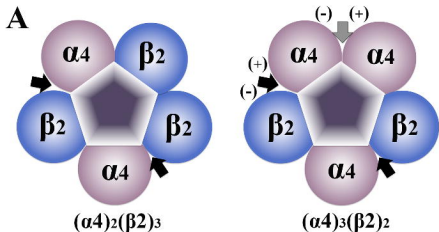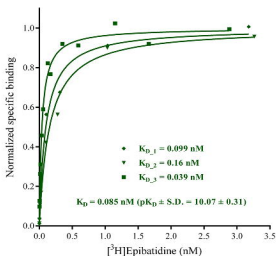
Ls-AChBP, *Ls*-AChBP^{HQT} and α4β2^{HQT}
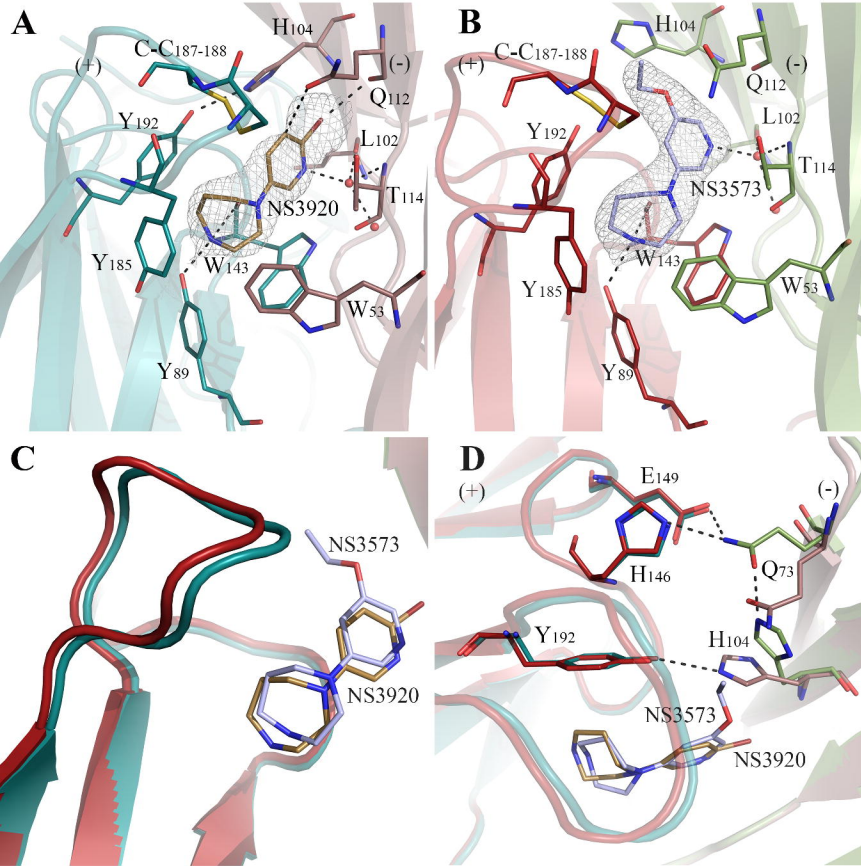
- AChBP
- AChBP^{HQT}
- α4β2
- α4β2^{HQT}
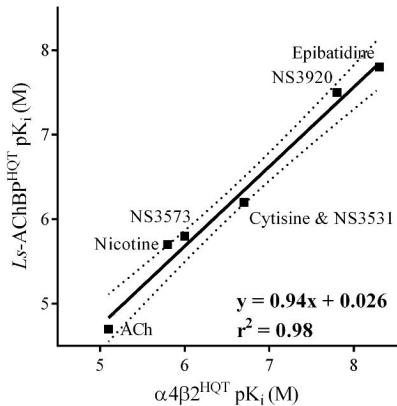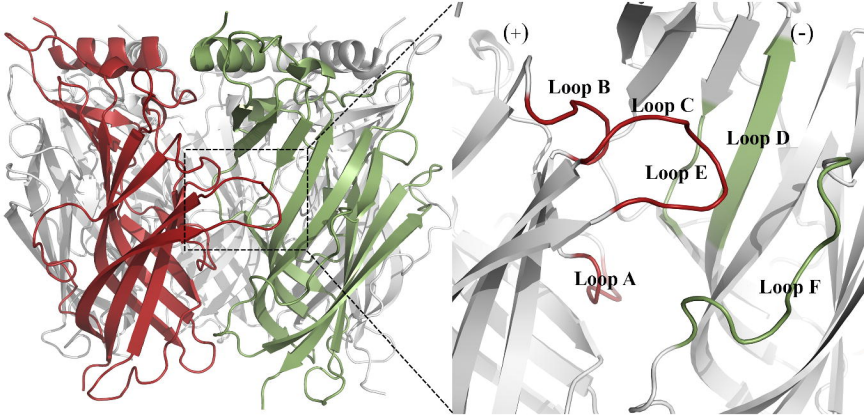
Figure 2
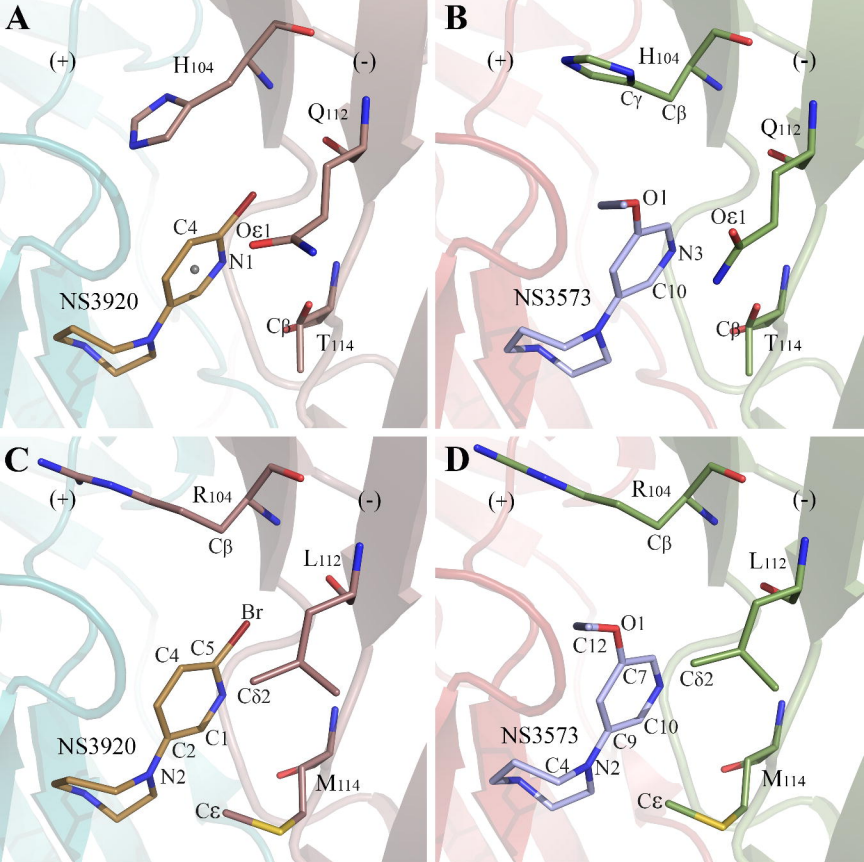
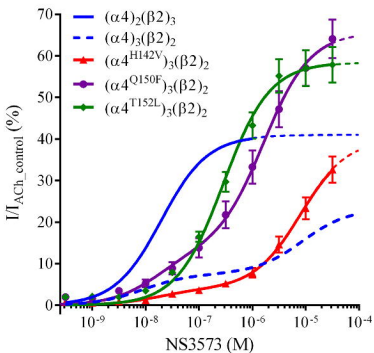**Figure 3**

Figure 4

Figure 5

Figure 6

A

Y-axis: $I/I_{ACh, control}$ (%)
X-axis: NS3920 (M)

Legend:
- $(\alpha 4)_2(\beta 2)_3$
- $(\alpha 4)_3(\beta 2)_2$
- $(\alpha 4^{H142V})_3(\beta 2)_2$
- $(\alpha 4^{Q150F})_3(\beta 2)_2$
- $(\alpha 4^{T152L})_3(\beta 2)_2$

B

Y-axis: $I/I_{ACh, control}$ (%)
X-axis: NS3573 (M)

Legend:
- $(\alpha 4)_2(\beta 2)_3$
- $(\alpha 4)_3(\beta 2)_2$
- $(\alpha 4^{H142V})_3(\beta 2)_2$
- $(\alpha 4^{Q150F})_3(\beta 2)_2$
- $(\alpha 4^{T152L})_3(\beta 2)_2$

Figure 7